

The influence of the $6s^2$ configuration of Bi^{3+} on the structures of $\text{A}'\text{BiNb}_2\text{O}_7$ ($\text{A}' = \text{Rb}, \text{Na}, \text{Li}$) layered perovskite oxides.

Subhadip Mallick, Guru Khalsa, Jeffrey Z. Kaaret, Weiguo Zhang, Maria Batuk, Alexandra S. Gibbs, Joke Hadermann, P. Shiv Halasyamani, Nicole A. Benedek, and Michael A. Hayward*

Table of contents

1. Structural Characterisation of $\text{RbBiNb}_2\text{O}_7$

Figure S1. Synchrotron X-ray powder diffraction data collected from $\text{RbBiNb}_2\text{O}_7$ in the range $8 < 2\theta < 14$, indexed using the reported lattice parameters of $\text{RbBiNb}_2\text{O}_7$ ($a = 5.463 \text{ \AA}$, $b = 5.393 \text{ \AA}$, $c = 11.232 \text{ \AA}$). The black arrows denote peaks which require a doubling of the c lattice parameter.

Figure S2. Observed, calculated and difference plots from the structural refinement of $\text{RbBiNb}_2\text{O}_7$ against synchrotron X-ray diffraction data collected at room temperature.

2. Structural Characterisation of $\text{LiBiNb}_2\text{O}_7$.

Figure S3. Synchrotron X-ray diffraction data collected from $\text{LiBiNb}_2\text{O}_7$. Presence of [012] and [016] peaks rules out the $Bb2_1m$ structural model. Peak marked with * is from a $(\text{Li/Rb})\text{NbO}_3$ impurity.

Table S1. Fitting statistics from the refinement of a series of structural models against the powder neutron diffraction data collected from $\text{LiBiNb}_2\text{O}_7$.

Table S2. Cation bond valence sums from the $P2cm$, constrained $P2cm$ and $B2cm$ structural models of $\text{LiBiNb}_2\text{O}_7$.

Figure S4. Observed, calculated and difference plots from the structural refinement of $\text{LiBiNb}_2\text{O}_7$ against synchrotron X-ray diffraction data.

3. Structural Characterisation of $\text{NaBiNb}_2\text{O}_7$.

Table S3. Fitting statistics from the refinement of different models against the powder neutron diffraction data collected from $\text{NaBiNb}_2\text{O}_7$.

Table S4. Cation bond valence sum calculated for the $P2_1nm$, constrained $P2_1nm$ and $Pnam$ models of $\text{NaBiNb}_2\text{O}_7$.

Table S5. Fitting statistics from the structural refinement, against NPD data, of a series of different models obtained by the addition of Γ -point distortion modes to the $Pnam$ structural model of $\text{NaBiNb}_2\text{O}_7$.

Table S6. Fractional coordinates and cation bond valence sums of from the structural refinement of a series of distorted non-centrosymmetric models against the powder neutron diffraction data collected from $\text{NaBiNb}_2\text{O}_7$.

Figure S5. Observed, calculated and difference plots from the structural refinement of $Pnam$, $P2_1am$ and $P2_12_12_1$ symmetry models against synchrotron X-ray diffraction data collected from $\text{NaBiNb}_2\text{O}_7$, showing the poor fits obtained by the $Pnam$, $P2_1am$ models.

Figure S6. Observed, calculated and difference plots from the structural refinement of a $P2_12_12_1$ model against synchrotron X-ray diffraction data collected from $\text{NaBiNb}_2\text{O}_7$.

Figure S7. Fit to NPD data collected from $\text{NaBiNb}_2\text{O}_7$ (top) without accounting for preferred orientation or anisotropic peak broadening; (middle) accounting for anisotropic broadening only; (bottom) accounting for both anisotropic peak broadening and preferred orientation.

4. Microstructural Characterisation of $\text{NaBiNb}_2\text{O}_7$.

Figure S8. HAADF-STEM image collected from $\text{NaBiNb}_2\text{O}_7$.

5. Distortion modes of $A'ANb_2O_7$ phases.

Table S7. Distortion mode amplitudes extracted from the refined structure of $RbNdNb_2O_7$ (space group $I2cm$) compared to the $P4/mmm$ symmetry aristotype structure.

Table S8. Distortion mode amplitudes extracted from the refined structure of $RbBiNb_2O_7$ (space group $I2cm$) compared to the $P4/mmm$ symmetry aristotype structure.

Table S9. Distortion mode amplitudes extracted from the refined structure of $LiNdNb_2O_7$ (space group $B2cm$) compared to the $I4/mmm$ symmetry aristotype structure.

Table S10. Distortion mode amplitudes extracted from the refined structure of $LiBiNb_2O_7$ (space group $B2cm$) compared to the $I4/mmm$ symmetry aristotype structure.

Table S11. Distortion mode amplitudes extracted from the refined structure of $NaBiNb_2O_7$ (space group $P2_12_12_1$) compared to the $I4/mmm$ symmetry aristotype structure.

6. First-principles analysis of $RbBiNb_2O_7$ and $LiBiNb_2O_7$.

Table S12. Comparison between theoretical and experimentally synthesized structures of $RbBiNb_2O_7$ in the polar $I2cm$ phase.

Table S13. Comparison between structures of $LiBiNb_2O_7$ in the listed space groups from our first-principles calculations (PBEsol) and experiment.

1. Structural Characterisation of RbBiNb₂O₇

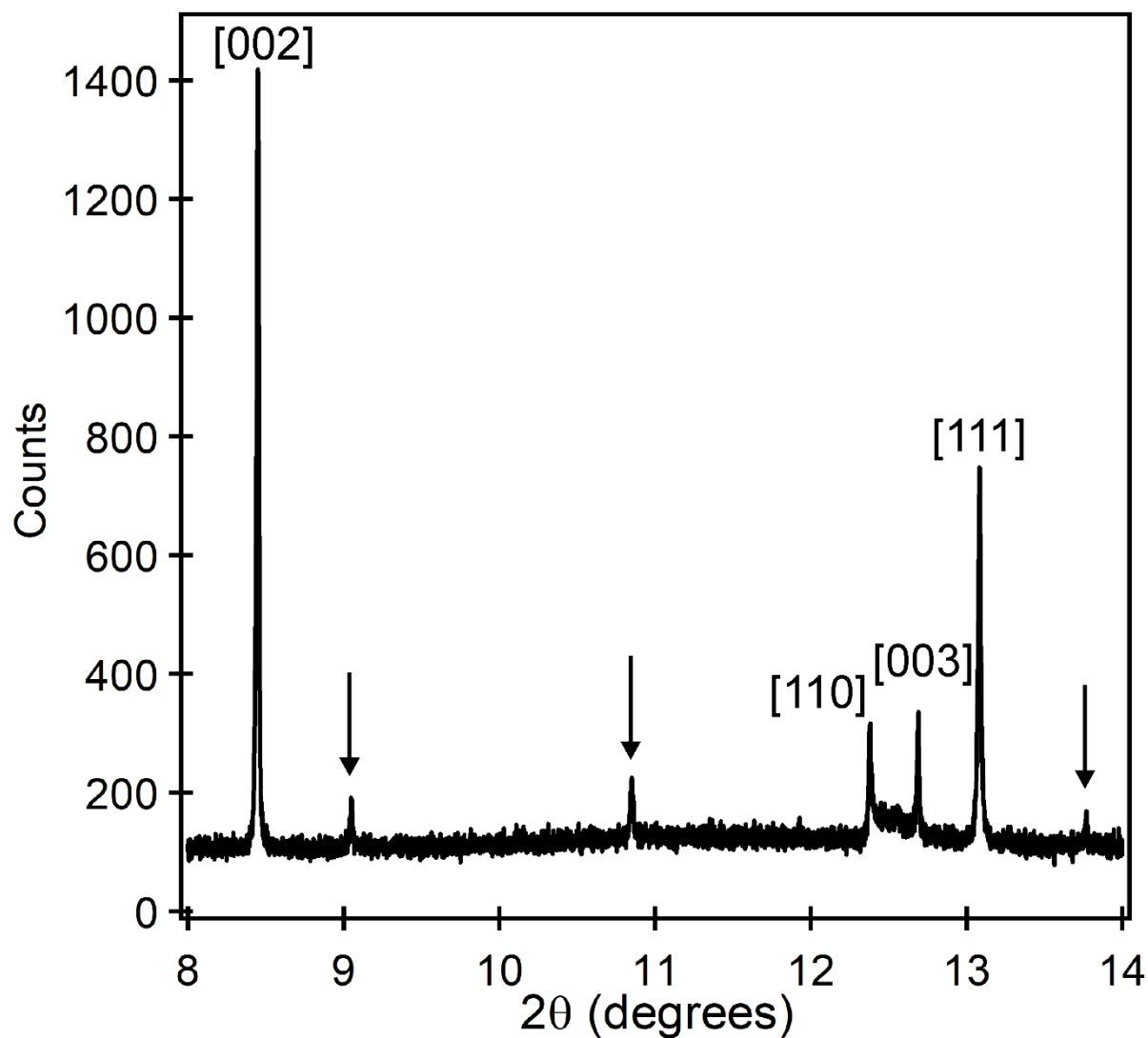


Figure S1. Synchrotron X-ray powder diffraction data collected from RbBiNb₂O₇ in the range $8 < 2\theta < 14$, indexed using the reported lattice parameters of RbBiNb₂O₇ ($a = 5.463 \text{ \AA}$, $b = 5.393 \text{ \AA}$, $c = 11.232 \text{ \AA}$). The black arrows denote peaks which require a doubling of the c lattice parameter.

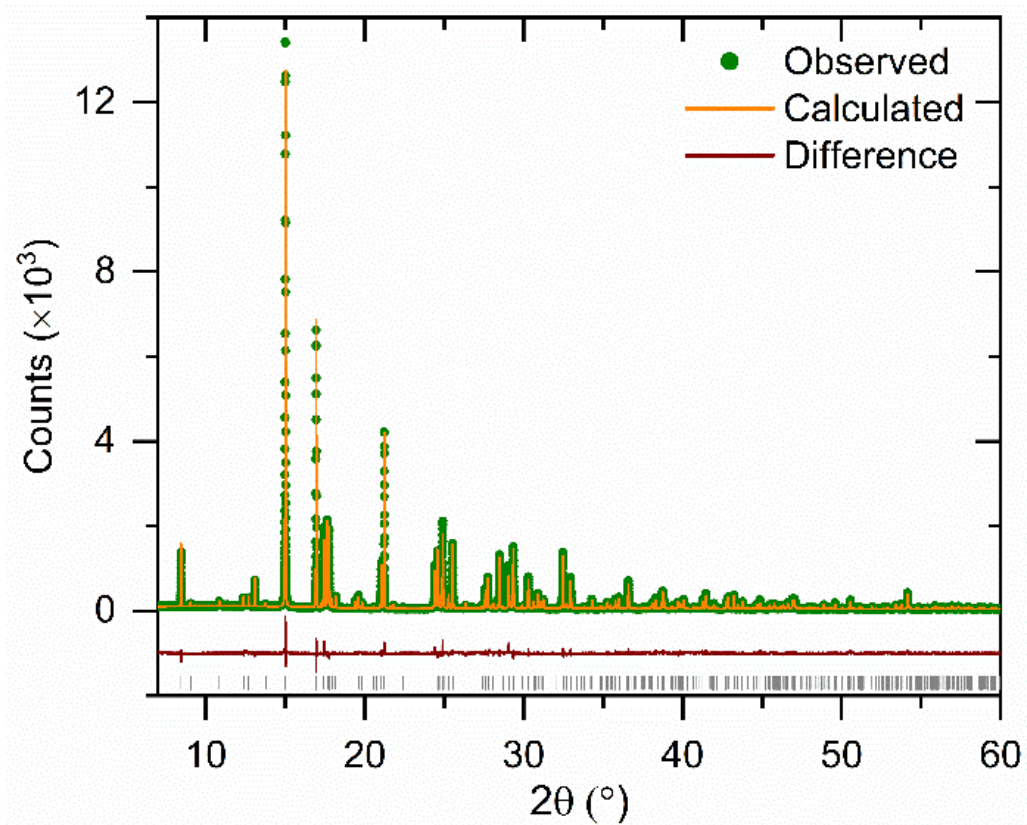


Figure S2. Observed, calculated and difference plots from the structural refinement of RbBiNb₂O₇ against synchrotron X-ray diffraction data collected at room temperature.

2. Structural Characterisation of LiBiNb₂O₇.

SXRD and PND data collected from LiBiNb₂O₇ at room temperature can be indexed using an orthorhombic unit cell ($a = 5.456 \text{ \AA}$, $b = 5.341 \text{ \AA}$, $c = 20.819 \text{ \AA}$) consistent with an $a' \approx \sqrt{2} \times a$, $b' \approx \sqrt{2} \times b$, $c' \approx c$ geometric expansion of the undistorted $n = 2$ Ruddlesden-Popper aristotype unit cell, directly analogous to the reported structure of LiNdNb₂O₇. Powder SHG measurements indicate LiBiNb₂O₇ exhibits an SHG activity ~ 2 times that of KDP (Figure 1 in the main text) and thus adopts non-centrosymmetric crystal structure. Symmetry analysis of the distortions of the $n = 2$ Ruddlesden-Popper framework indicates that there are four non-centrosymmetric candidate structures described in space groups $Bb2_1m$, $P2_1nm$, $B2cm$ and $P2cm$ respectively.

Further examination of diffraction data allowed us to eliminate the $Bb2_1m$ structure based on extinction conditions, as shown in Figure S3. Thus, structural models were constructed for LiBiNb₂O₇ based on the distortions described in space groups $P2_1nm$, $B2cm$ and $P2cm$ and these models were refined against the NPD data collected at room temperature. Refinement of $P2_1nm$ model results in a significantly worse fit to the data than either $B2cm$ or $P2cm$ models as detailed in Table S1, and so this model was eliminated.

The Li⁺ cations in cation-exchanged LiAB₂O₇ Ruddlesden-Popper phases occupy only half of the available pseudo-tetrahedral coordination sites in the framework, so can adopt either ordered or disordered arrangements. Refinement of lithium ordered and disordered models against the PND data revealed that ordered models give superior fits compared to disordered models for both the $B2cm$ and $P2cm$ distorted structures. The refinement parameters shown in Table S1 indicate a slightly better fit for the unconstrained $P2cm$ model compared to the $B2cm$ model. However, examination of the unconstrained $P2cm$ model reveals that it has twice as many atoms in the asymmetric unit as the $B2cm$ model and that when refined against the NPD data, chemically equivalent atoms in the $P2cm$ model move to very different local environments. As a result, bond valence sums (BVS) calculated for pairs of chemically equivalent cations in the BiNb₂O₇ perovskite blocks are very different (Table S2) making the resulting structure chemically implausible. To address this situation, we added constrains to the $P2cm$ model to make the environments of the two niobium cations more similar, following the procedure adopted during the refinement of LiNdNb₂O₇.¹ This more symmetric $P2cm_{\text{constrained}}$ model fits the data more poorly than the $B2cm$ model as shown in Table S1, confirming that LiBiNb₂O₇ adopts an $a^-a^-c^+/(a^-a^-c^+)$ distorted $n = 2$ Ruddlesden-Popper structure, described in space group $B2cm$ analogous to that reported for LiNdNb₂O₇.

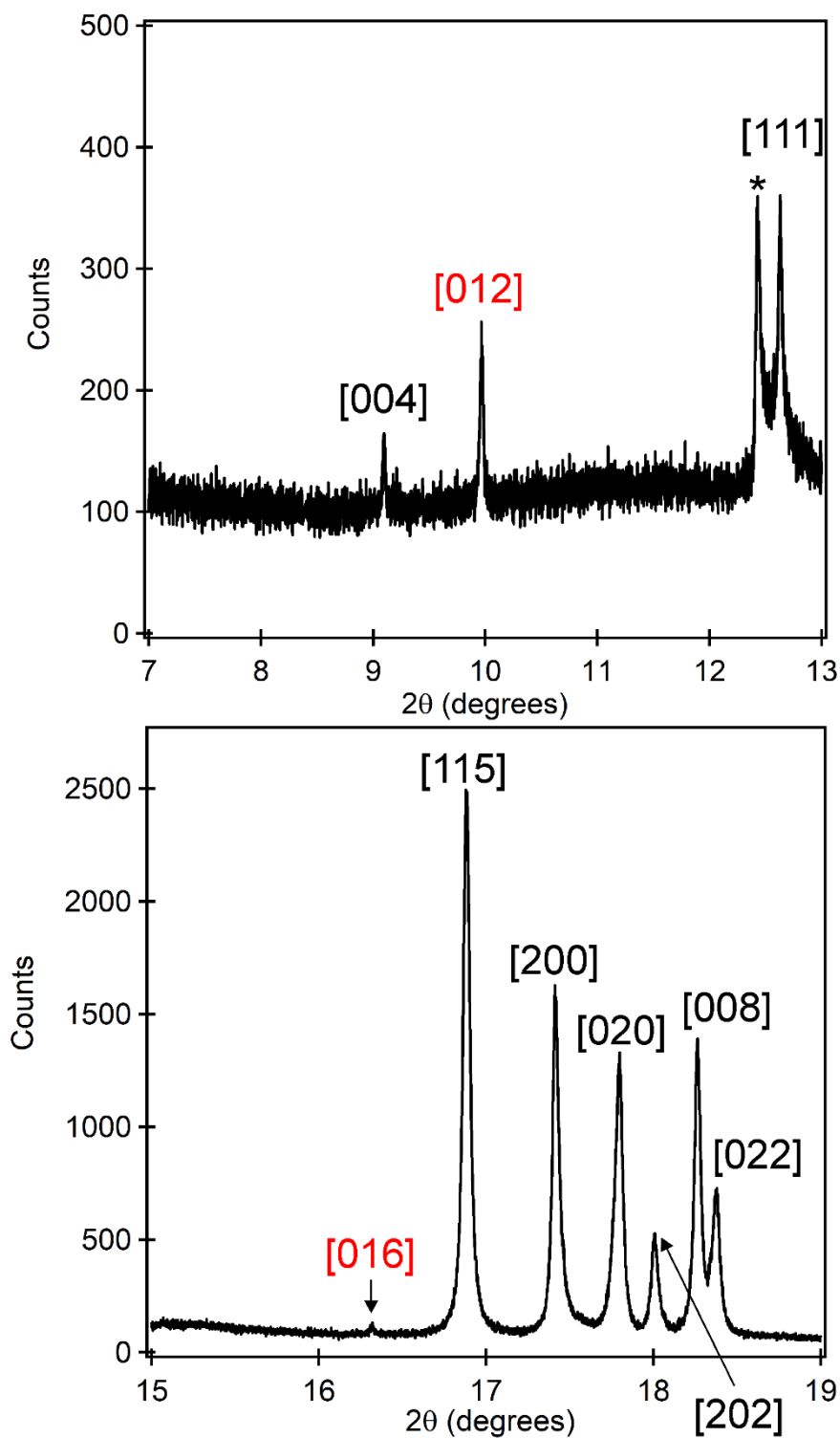


Figure S3. Synchrotron X-ray diffraction data collected from $\text{LiBiNb}_2\text{O}_7$. Presence of [012] and [016] peaks rules out the $Bb2_1m$ structural model. Peak marked with * is from a $(\text{Li/Rb})\text{NbO}_3$ impurity.

Space group	Tilt system	Glazer tilt	#parameters	R _p (%)	wR _p (%)
<i>P2₁nm</i>	$\Phi_1\Phi_2\Psi_z/\Phi_2\Phi_1\Psi_z$	$a^-b^-c^+/b^-a^-c^+$	128	7.645	9.081
<i>B2cm</i>	$\Phi\Phi\Psi_z/-(\Phi\Phi\Psi_z)$	$a^-a^-c^+/-(a^-a^-c^+)$	96	5.368	6.924
<i>P2cm</i>	$\Phi_1\Phi_2\Psi_z/-(\Phi_1\Phi_2)\Psi_z$	$a^-b^-c^+/-(a^-b^-)c^+$	120	4.870	5.773
<i>P2cm</i> _{constrained}	$\Phi_1\Phi_2\Psi_z/-(\Phi_1\Phi_2)\Psi_z$	$a^-b^-c^+/-(a^-b^-)c^+$	117	6.464	7.776

Table S1. Fitting statistics from the refinement of a series of structural models against the powder neutron diffraction data collected from LiBiNb₂O₇.

	<i>P2cm</i>	<i>P2cm</i> _{constrained}	<i>B2cm</i>
Li1	0.98	0.99	0.97
Li2	1.02	1.05	
Bi1	2.42	2.40	3.00
Bi2	3.53	3.18	
Nb1	4.55	5.03	5.03
Nb2	1.52	5.12	

Table S2. Cation bond valence sums from the *P2cm*, constrained *P2cm* and *B2cm* structural models of LiBiNb₂O₇.

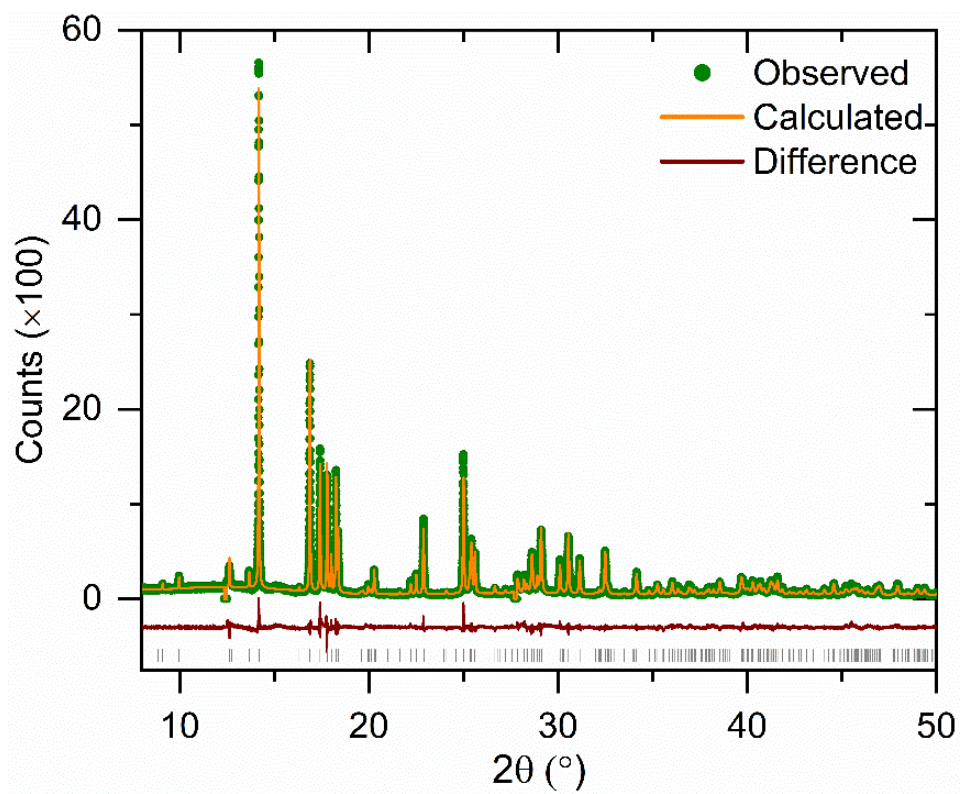


Figure S4. Observed, calculated and difference plots from the structural refinement of $\text{LiBiNb}_2\text{O}_7$ against synchrotron X-ray diffraction data.

3. Structural Characterisation of NaBiNb₂O₇.

High-resolution SXRD and PND data collected from NaBiNb₂O₇ can be indexed using an orthorhombic unit cell ($a = 5.47 \text{ \AA}$, $b = 5.38 \text{ \AA}$, $c = 21.67 \text{ \AA}$) which is consistent with an $a' \approx \sqrt{2} \times a$, $b' \approx \sqrt{2} \times b$, $c' \approx c$ geometric expansion of the undistorted aristotype unit cell of an $n = 2$ Ruddlesden-Popper structure. The extinction conditions observed in the SXRD and NPD data allow us to eliminate the majority of $n = 2$ Ruddlesden-Popper phases distorted by cooperative tilting on the NbO₆ units¹ leaving 5 candidate structures described in space groups *Pbcm*, *Pnnm*, *Pnam*, *P2₁nm* and *P2cm*.

Models of these distorted structures were constructed and refined against the NPD data. The model described in space group *P2₁nm* gave the best fit to the data (Table S3). However, close inspection of the refined *P2₁nm* model reveals that the resulting structure is very irregular, with chemically equivalent cations having very different local bonding environments, as evident from the bond valence sums of the metal cations (Table S4). To address this problem, constraints were added to the model to make the bond valence sums of chemically equivalent cations the same, resulting in a poor fit to the NPD data as noted in Table S3, so this model was discarded.

The model described in space group *Pnam* gives the best fit to the data of the remaining models as shown in Table S3, and yields a chemically reasonable structure. However, this model is centrosymmetric (incompatible with observed SHG activity), suggesting that it describes the tilting distortion of the NbO₆ units accurately, but the 'true' structure of NaBiNb₂O₇ is subject to a further distortion which breaks the inversion symmetry of this *Pnam* model. Thus we considered the inclusion of Γ -point distortion modes in the *Pnam* model with the help of the ISODISTORT software.² This symmetry analysis yields four candidate non-centrosymmetric models described in space groups *P2₁2₁2₁*, *Pn2₁m*, *P2₁am* and *Pna2₁*. Fitting statistics from the refinement of these four non-centrosymmetric models (Table S5) are comparable to one another. We therefore examined the refined structures to see if they were chemically reasonable.

***Pn2₁m* model:** There are 2 sites for Na, Bi and Nb in the *Pn2₁m* model. The Na site occupancies were refined within the constraint of total composition being NaBiNb₂O₇, to establish if the Na⁺ cations were ordered over the two sites. After refinement, the occupancy of one site reached 0.68 and the other 0.32. As the Na ordering is not significant we continued further analysis with this level of ordering. Examining the refined models, it can be seen in Table S6 that the two Bi sites have very different bond valence sum values, and the fitting statistics for this model are the poorest of the 4 considered, so this structure was discarded.

***Pna2₁* model:** There are 2 sites for Na and Nb and one site for Bi in this model. The Na site occupancies were refined within the constraint of total composition being NaBiNb₂O₇, to establish if the Na⁺ cations were ordered over the two sites. The occupancy of one site moves to 0.81 and the other site to 0.19, indicating the Na⁺ cations are ordered. The site with 0.81 occupancy was fixed as fully occupied which did not alter the fitting statistics significantly. In the final refined structure, we observe that the two chemically equivalent Nb sites have very different local bonding environments which result in significantly different bond valence sum values (Table S6) which make the structure chemically implausible and thus so model was discarded.

***P2₁am* model:** There are two sites for Na, Nb and Bi in this model. The Na site occupancies were refined within the constraint of total composition being NaBiNb₂O₇, to establish if the Na⁺ cations were ordered over the two sites. The occupancy of one site moves to 0.88 and the other site to 0.12, indicating the Na⁺ cations are ordered. The site with 0.88 occupancy was fixed to be fully occupied which did not alter the fitting statistics significantly. Table S6 reveals that the bond valence sums of chemically equivalent Bi and Nb cations are significantly different from one another in the final refined structure. Close inspection reveals that the Bi1 and Nb1 sites belong to one Nb₂O₇ layer and Bi2 and Nb2 belong to another Nb₂O₇ layer. This allows the structure to have a very irregular local bonding environment for these chemically equivalent cations. From the Cartesian coordinates and bond valence sum values of the two Bi sites, it is clear that they are uneven and if this were the true structure we would be able to distinguish them in high-resolution X-ray powder diffraction given the strong X-ray scattering power of bismuth. Indeed, we observe that the a calculated X-ray powder diffraction pattern of this *P2₁am* structure yields calculated intensities that are not observed in the experimental X-ray powder diffraction pattern as shown in Figure S5. For these reasons, the *P2₁am* model was discarded.

***P2₁2₁2₁* model:** There are two independent sites for Na and Nb and one site for Bi in this model. The Na site occupancies were refined within the constraint of total composition being NaBiNb₂O₇, to establish if the Na⁺ cations were ordered over the two sites. The occupancy of one site moves to 0.88 and the other site to 0.12, indicating the Na⁺ cations are ordered. The site with occupancy 0.88 was fixed to be completely occupied which did not alter the fitting statistics significantly. Bond valence sums of the chemically equivalent cations in the refined structure (Table S6) are similar to one another and close to their ideal value. Furthermore, the *P2₁2₁2₁* model allows the 'checkerboard' ordering of Na, which minimizes the Na-Na repulsion as evident from the large Na-Na distance (3.77 Å). For these reasons the *P2₁2₁2₁* model is thought to be the best description of the structure of NaBiNb₂O₇. In the final cycles of

refinement the occupancy of the Na cation site was allowed to deviate from full occupancy to yield a value of 0.81(4), without any significant changes to any other structural parameters.

It was observed that the both the SXRD and NPD data collected from NaBiNb₂O₇ exhibited strong (00 l) preferred orientation and hkl -dependent peak broadening. The preferred orientation was modelled using an 4th order spherical harmonic expression,³ and the anisotropic peak broadening was modelled using an anisotropic line-shape broadening function described by Stephens⁴. Figure S7 shows the effect of these contributions.

Space group	Tilt system	Glazer tilt	#parameters	R _p (%)	wR _p (%)
<i>Pbcm</i> (#57)	$\Phi\Phi\Psi_z/-(\Phi\Phi)\Psi_z$	$a^-a^-c^+/- (a^-a^-)c^+$	96	7.556	8.019
<i>Pnmm</i> (#58)	$\Phi_1\Phi_2 0/ \Phi_2\Phi_1 0$	$a^-b^-c^0/b^-a^-c^0$	98	7.848	8.114
<i>Pnam</i> (#62)	$\Phi\Phi\Psi_z/ \Phi\Phi-\Psi_z$	$a^-a^-c^+/a^-a^-c^+$	98	6.366	6.635
<i>P2₁nm</i> (#31)	$\Phi_1\Phi_2\Psi_z/ \Phi_2\Phi_1\Psi_z$	$a^-b^-c^+/b^-a^-c^+$	118	5.840	6.127
<i>P2₁nm</i> _{constrained}	$\Phi_1\Phi_2\Psi_z/ \Phi_2\Phi_1\Psi_z$	$a^-b^-c^+/b^-a^-c^+$	105	7.405	7.700
<i>P2cm</i> (#28)	$\Phi_1\Phi_2\Psi_z/-(\Phi_1\Phi_2)\Psi_z$	$a^-b^-c^+/- (a^-b^-)c^+$	116	7.633	8.028

Table S3. Fitting statistics from the refinement of different models against the powder neutron diffraction data collected from NaBiNb₂O₇.

	<i>P2₁nm</i>	<i>P2₁nm</i> _{constrained}	<i>Pnam</i>
Bi1	2.138	2.671	2.948
Bi2	3.722	3.184	
Nb1	4.697	5.033	4.908
Nb2	5.513	4.900	

Table S4. Cation bond valence sum calculated for the *P2₁nm*, constrained *P2₁nm* and *Pnam* models of NaBiNb₂O₇.

Space group	Distortion mode	#parameters	R _p (%)	wR _p (%)	Na ordering pattern
<i>Pnam</i> (#62)		98	6.37	6.63	Disordered
<i>Pn2₁m</i> (#31)	Γ_2^-	119	6.50	5.56	Checkerboard
<i>Pna2₁</i> (#33)	Γ_4^-	112	6.05	6.29	Stripes
<i>P2₁am</i> (#26)	Γ_3^-	114	5.23	5.37	Stripes
<i>P2₁2₁2₁</i> (#19)	Γ_1^-	111	6.13	6.35	Checkerboard

Table S5. Fitting statistics from the structural refinement, against NPD data, of a series of different models obtained by the addition of Γ -point distortion modes to the *Pnam* structural model of NaBiNb₂O₇.

<i>Pnam</i>				
	<i>x</i>	<i>y</i>	<i>z</i>	BVS
Na	0.9984(22)	0.2568(27)	0.4908(8)	+1.037
Bi	0.6917(6)	0.0237(7)	0.25	+2.948
Nb	0.7538(5)	0.0139(5)	0.8583(1)	+4.908
<i>P2₁2₁2₁</i>				
Na	0.991(2)	0.995(3)	0.5047(9)	+0.989
Bi	0.6936(6)	0.2716(7)	0.2510(8)	+2.960
Nb1	0.7481(12)	0.2610(20)	0.8630(4)	+4.863
Nb2	0.2420(11)	0.2330(20)	0.1439(4)	+5.092
<i>Pn2₁m</i>				
Na1	0.7197(23)	0.6986(25)	0.2603(7)	+1.183
Na2	0.4945(65)	0.5650(37)	0.6947(15)	+1.105
Bi1	0.4891(21)	0.9247(15)	0.0000	+2.723
Bi2	0.9216(13)	0.4949(16)	0.0000	+3.196
Nb1	0.5152(13)	0.9474(10)	0.6117(3)	+5.112
Nb2	0.0007(13)	0.4839(8)	0.3953(3)	+5.081
<i>P2₁am</i>				
Na	0.9761(21)	0.4855(20)	0.2502(6)	+1.010
Bi1	0.3110(14)	0.7135(13)	0.0000	+3.650
Bi2	0.8075(14)	0.7737(13)	0.0000	+2.481
Nb1	0.2328(10)	0.7412(11)	0.6135(2)	+4.871
Nb2	0.7486(9)	0.7655(11)	0.1033(2)	+5.183
<i>Pna2₁</i>				
Na	0.4957(25)	0.7522(31)	0.0026(10)	+0.859
Bi	0.6870(6)	0.9816(7)	0.7621(6)	+2.950
Nb1	0.7553(17)	0.9794(10)	0.1470(2)	+5.472
Nb2	0.2549(18)	0.5168(14)	0.3651(2)	+4.683

Table S6. Fractional coordinates and cation bond valence sums of from the structural refinement of a series of distorted non-centrosymmetric models against the powder neutron diffraction data collected from NaBiNb₂O₇.

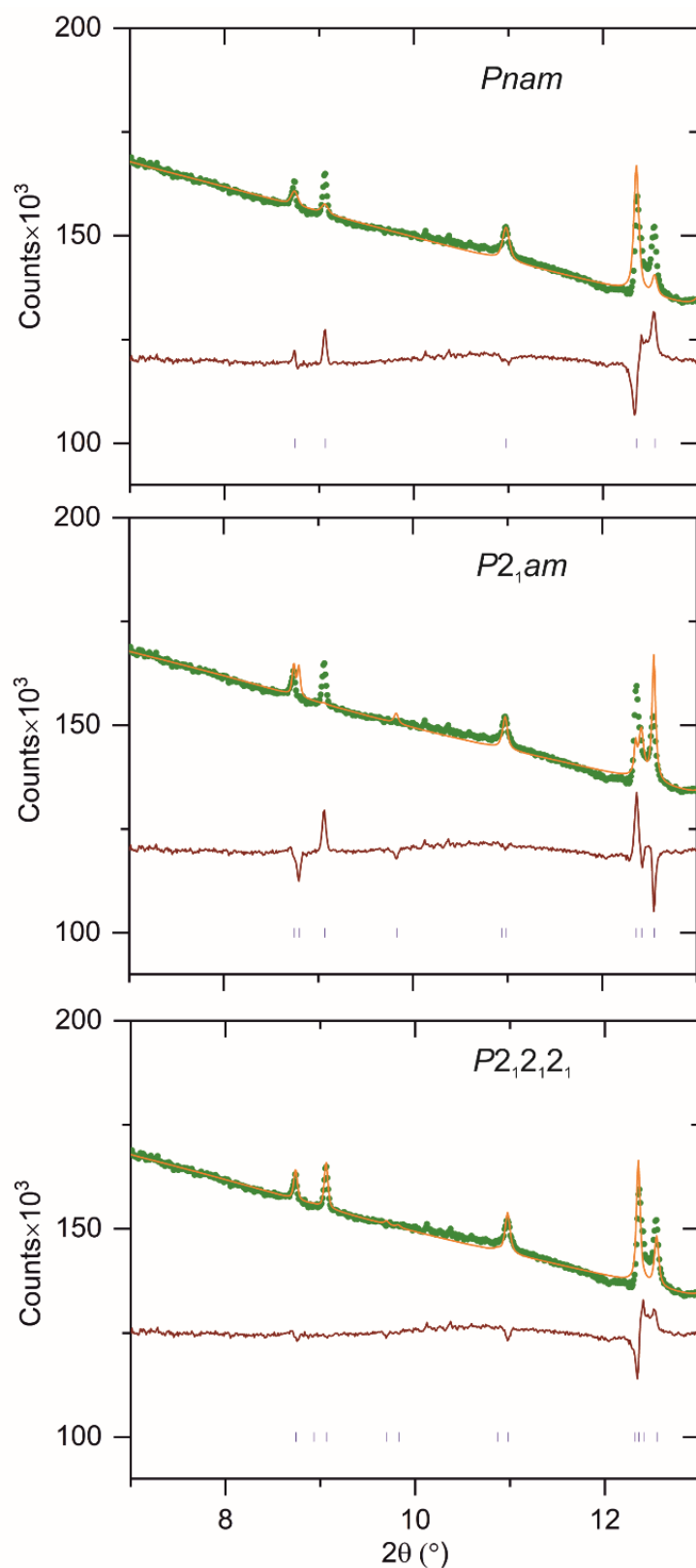


Figure S5. Observed, calculated and difference plots from the structural refinement of $Pnam$, $P2_1am$ and $P2_12_12_1$ symmetry models against synchrotron X-ray diffraction data collected from $\text{NaBiNb}_2\text{O}_7$, showing the poor fits obtained by the $Pnam$, $P2_1am$ models.

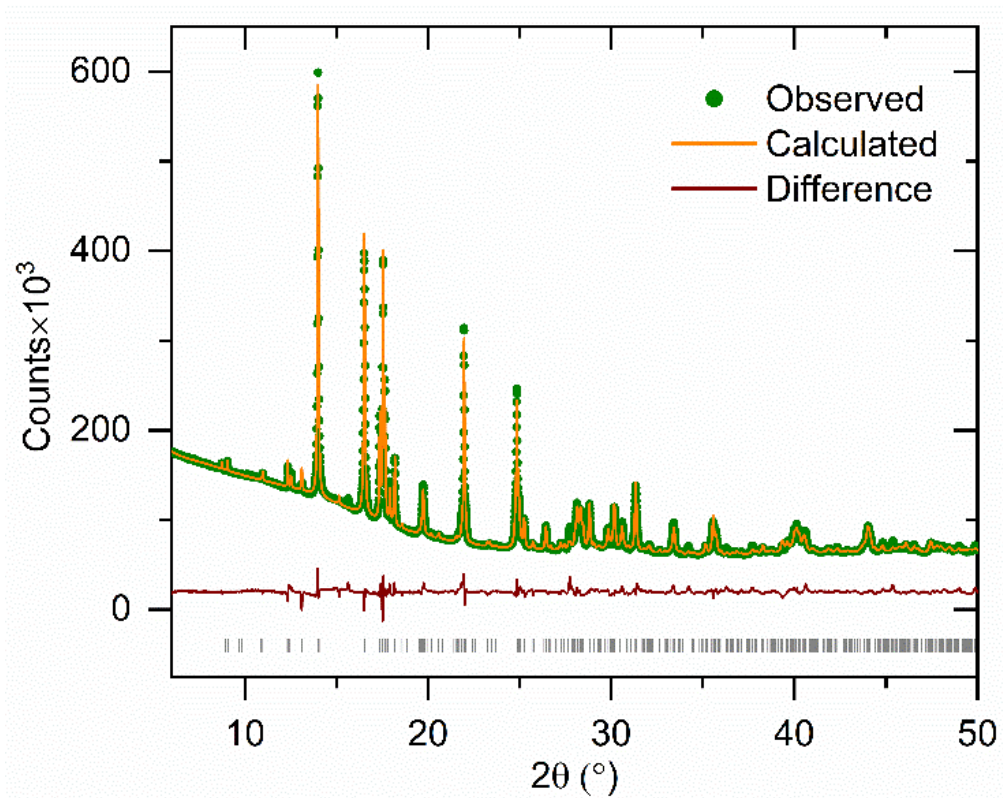


Figure S6. Observed, calculated and difference plots from the structural refinement of a *P*2₁2₁2₁ model against synchrotron X-ray diffraction data collected from NaBiNb₂O₇.

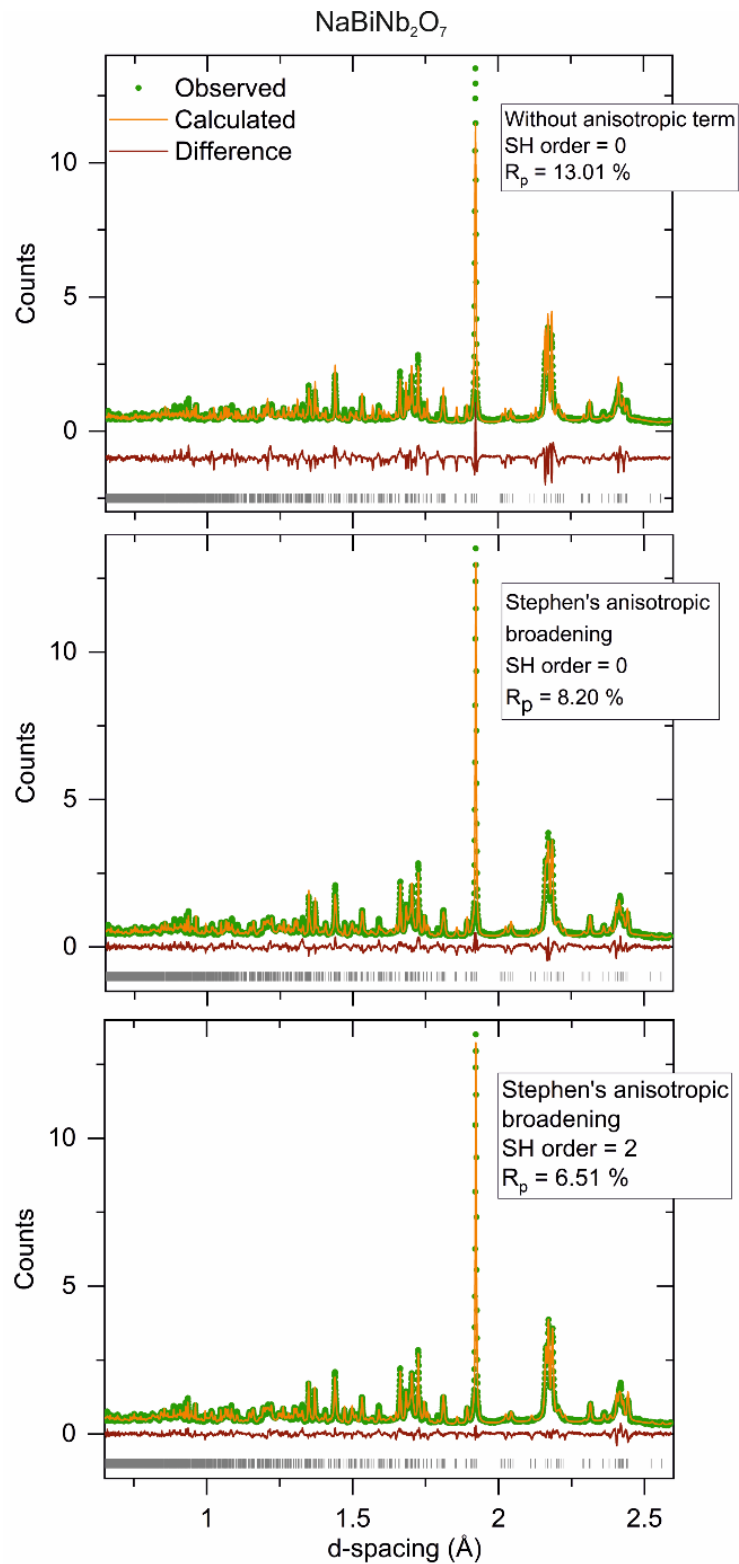


Figure S7. Fit to NPD data collected from $\text{NaBiNb}_2\text{O}_7$ (top) without accounting for preferred orientation or anisotropic peak broadening; (middle) accounting for anisotropic broadening only; (bottom) accounting for both anisotropic peak broadening and preferred orientation.

4. Microstructural Characterisation of NaBiNb₂O₇.

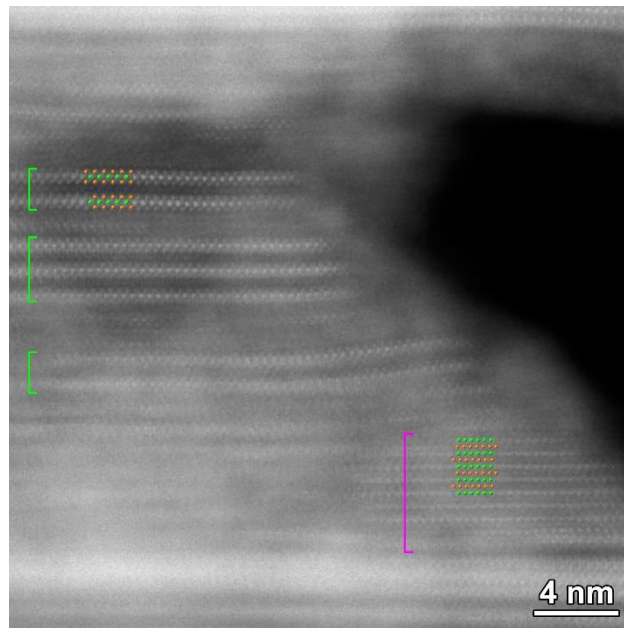


Figure S8. HAADF-STEM image collected from NaBiNb₂O₇. Green brackets outline the thin slabs of a Dion-Jacobson phase with [010] orientation. Pink bracket [001] or [101] zone of BiNbO₄ (Pnna, $a = 5.68 \text{ \AA}$, $b = 11.72 \text{ \AA}$, $c = 4.98 \text{ \AA}$). The models are inserted: green – Bi, orange – Nb, blue – Na.

5. Distortion modes of $A'ANb_2O_7$ phases.

The structures of the $A'ANb_2O_7$ phases can be analysed in terms of the distortion modes which need to be applied to the undistorted aristotype structures to obtain the observed experimental structures. The atom displacements, which occur on going from the aristotype structure to the distorted structure, can be deconvoluted into contributions from the individual distortion modes.² The data tabulated below reports the amplitudes of the displacements due to the distortion modes in three ways:

A_s : the supercell normalised amplitude, which is the square root of the sum of the squares of the mode-induced displacements.

A_p : the parent cell normalised amplitude. $A_p = A_s \sqrt{V_p/V_s}$, where V_p and V_s are the volumes of the parent cell and supercell respectively.

d_{max} is the maximum displacement experienced by an atom due to this distortion mode.

RbNdNb ₂ O ₇			
Distortion mode	A_s	A_p	d_{max} (Å)
[0,0,0] Γ_1^+ [Nb1:h:dsp] A1(a)	0.06720	0.04752	0.03360
[0,0,0] Γ_1^+ [O1:i:dsp] A1(a)	0.24133	0.17065	0.08532
[0,0,0] Γ_1^+ [O2:h:dsp] A1(a)	0.11508	0.08137	0.05754
[0,0,0] Γ_1^+ all	0.27568	0.19494	
[0,0,0] Γ_5^- [Rb1:b:dsp] Eu(a)	0.0000	0.0000	0.0000
[0,0,0] Γ_5^- [Nd1:a:dsp] Eu(a)	0.01537	0.01087	0.01087
[0,0,0] Γ_5^- [Nb1:h:dsp] E(a)	-0.07282	-0.05149	0.03641
[0,0,0] Γ_5^- [O1:i:dsp] B2(a)	0.53204	0.37621	0.18810
[0,0,0] Γ_5^- [O1:i:dsp] B1(a)	0.12119	0.08569	0.04285
[0,0,0] Γ_5^- [O2:h:dsp] E(a)	-0.08043	-0.05687	0.04022
[0,0,0] Γ_5^- [O3:c:dsp] Eu(a)	-0.25286	-0.17880	0.17880
[0,0,0] Γ_5^- all	0.61131	0.43226	
$[\frac{1}{2}, \frac{1}{2}, \frac{1}{2}] A_2^+$ [O1:i:dsp] B2(a)	-0.72225	-0.51071	0.25535
$[\frac{1}{2}, \frac{1}{2}, \frac{1}{2}] A_2^+$ all	0.72225	0.51071	
$[\frac{1}{2}, \frac{1}{2}, \frac{1}{2}] A_3^+$ [O1:i:dsp] B1(a)	-0.10054	-0.07109	0.03555
$[\frac{1}{2}, \frac{1}{2}, \frac{1}{2}] A_3^+$ all	0.10054	0.07109	
$[\frac{1}{2}, \frac{1}{2}, \frac{1}{2}] A_5^-$ [Nd1:a:dsp] Eu(a)	-0.00769	-0.00544	0.00544
$[\frac{1}{2}, \frac{1}{2}, \frac{1}{2}] A_5^-$ [Nb1:h:dsp] E(a)	0.00978	0.00692	0.00489
$[\frac{1}{2}, \frac{1}{2}, \frac{1}{2}] A_5^-$ [O1:i:dsp] A1(a)	-0.76748	-0.54269	0.27135
$[\frac{1}{2}, \frac{1}{2}, \frac{1}{2}] A_5^-$ [O2:h:dsp] E(a)	-0.57280	-0.40503	0.28640
$[\frac{1}{2}, \frac{1}{2}, \frac{1}{2}] A_5^-$ [O3:c:dsp] Eu(a)	0.56182	0.39727	0.39727
$[\frac{1}{2}, \frac{1}{2}, \frac{1}{2}] A_5^-$ all	1.1104	0.78515	

Table S7. Distortion mode amplitudes extracted from the refined structure of RbNdNb₂O₇ (space group $I2cm$)⁵ compared to the $P4/mmm$ symmetry aristotype structure.

RbBiNb ₂ O ₇			
Distortion mode	A _s	A _p	d _{max} (Å)
[0,0,0] Γ_1^+ [Nb1:h:dsp] A1(a)	0.25562	0.18075	0.12781
[0,0,0] Γ_1^+ [O1:i:dsp] A1(a)	0.31711	0.22423	0.11212
[0,0,0] Γ_1^+ [O2:h:dsp] A1(a)	0.19732	0.13953	0.09866
[0,0,0] Γ_1^+ all	0.45259	0.32003	
[0,0,0] Γ_5^- [Rb1:b:dsp] Eu(a)	0.0000	0.0000	0.0000
[0,0,0] Γ_5^- [Bi1:a:dsp] Eu(a)	-0.29270	-0.20697	0.20697
[0,0,0] Γ_5^- [Nb1:h:dsp] E(a)	0.11920	0.08429	0.05960
[0,0,0] Γ_5^- [O1:i:dsp] B2(a)	0.62795	0.44403	0.22201
[0,0,0] Γ_5^- [O1:i:dsp] B1(a)	0.22485	0.15899	0.07950
[0,0,0] Γ_5^- [O2:h:dsp] E(a)	0.12570	0.08888	0.06285
[0,0,0] Γ_5^- [O3:c:dsp] Eu(a)	0.34480	0.24381	0.24381
[0,0,0] Γ_5^- all	0.82429	0.58286	
[$\frac{1}{2}, \frac{1}{2}, \frac{1}{2}$] A ₂ ⁺ [O1:i:dsp] B2(a)	-0.73305	-0.51834	0.25917
[$\frac{1}{2}, \frac{1}{2}, \frac{1}{2}$] A ₂ ⁺ all	0.73305	0.51834	
[$\frac{1}{2}, \frac{1}{2}, \frac{1}{2}$] A ₃ ⁺ [O1:i:dsp] B1(a)	-0.04605	-0.03256	0.01628
[$\frac{1}{2}, \frac{1}{2}, \frac{1}{2}$] A ₃ ⁺ all	0.04605	0.03256	
[$\frac{1}{2}, \frac{1}{2}, \frac{1}{2}$] A ₅ ⁻ [Bi1:a:dsp] Eu(a)	0.12872	0.09102	0.09102
[$\frac{1}{2}, \frac{1}{2}, \frac{1}{2}$] A ₅ ⁻ [Nb1:h:dsp] E(a)	-0.05201	-0.03678	0.02601
[$\frac{1}{2}, \frac{1}{2}, \frac{1}{2}$] A ₅ ⁻ [O1:i:dsp] A1(a)	-0.45980	-0.32513	0.16256
[$\frac{1}{2}, \frac{1}{2}, \frac{1}{2}$] A ₅ ⁻ [O2:h:dsp] E(a)	-0.33483	-0.23676	0.16742
[$\frac{1}{2}, \frac{1}{2}, \frac{1}{2}$] A ₅ ⁻ [O3:c:dsp] Eu(a)	0.53406	0.37764	0.37764
[$\frac{1}{2}, \frac{1}{2}, \frac{1}{2}$] A ₅ ⁻ all	0.79248	0.56037	

Table S8. Distortion mode amplitudes extracted from the refined structure of RbBiNb₂O₇ (space group *I2cm*) compared to the *P4/mmm* symmetry aristotype structure.

LiNdNb ₂ O ₇			
Distortion mode	A _s	A _p	d _{max} (Å)
[0,0,0] Γ_1^+ [Nb1:e:dsp] A1(a)	-0.44990	-0.31813	0.22495
[0,0,0] Γ_1^+ [O2:g:dsp] A1(a)	-0.46851	-0.33129	0.16564
[0,0,0] Γ_1^+ [O3:e:dsp] A1(a)	0.67894	0.48008	0.33947
[0,0,0] Γ_1^+ all	0.93961	0.66441	
[0,0,0] Γ_5^- [Li1:d:dsp] E(a)	0	0	0
[0,0,0] Γ_5^- [Nd1:a:dsp] Eu(a)	0.03605	0.02549	0.02549
[0,0,0] Γ_5^- [Nb1:e:dsp] E(a)	0.24514	0.17334	0.12257
[0,0,0] Γ_5^- [O1:b:dsp] Eu(a)	0.21859	0.15457	0.15457
[0,0,0] Γ_5^- [O2:g:dsp] B2(a)	0.70126	0.49587	0.24793
[0,0,0] Γ_5^- [O2:g:dsp] B1(a)	0.38670	0.27344	0.13672
[0,0,0] Γ_5^- [O3:e:dsp] E(a)	0.20718	0.14650	0.10359
[0,0,0] Γ_5^- all	0.89073	0.62984	
[$\frac{1}{2}, \frac{1}{2}, 0$] X_2^+ [Li1:d:dsp] E(a)	0.44473	0.31447	0.22236
[$\frac{1}{2}, \frac{1}{2}, 0$] X_2^+ [O2:g:dsp] B2(a)	-0.66438	-0.46979	0.23489
[$\frac{1}{2}, \frac{1}{2}, 0$] X_2^+ [O2:g:dsp] B1(a)	0.01573	0.01112	0.00556
[$\frac{1}{2}, \frac{1}{2}, 0$] X_2^+ all	0.79965	0.56543	
[$\frac{1}{2}, \frac{1}{2}, 0$] X_4^- [Nd1:a:dsp] Eu(a)	0.01534	0.01085	0.01085
[$\frac{1}{2}, \frac{1}{2}, 0$] X_4^- [Nb1:e:dsp] E(a)	-0.01952	-0.01380	0.00976
[$\frac{1}{2}, \frac{1}{2}, 0$] X_4^- [O1:b:dsp] Eu(a)	0.52233	0.36934	0.36934
[$\frac{1}{2}, \frac{1}{2}, 0$] X_4^- [O2:g:dsp] A1(a)	0.79821	0.56442	0.28221
[$\frac{1}{2}, \frac{1}{2}, 0$] X_4^- [O3:e:dsp] E(a)	-0.96105	-0.67956	0.48052
[$\frac{1}{2}, \frac{1}{2}, 0$] X_4^- all	1.3543	0.95765	

Table S9. Distortion mode amplitudes extracted from the refined structure of LiNdNb₂O₇ (space group *B2cm*)¹ compared to the *I4/mmm* symmetry aristotype structure.

LiBiNb ₂ O ₇			
Distortion mode	A _s	A _p	d _{max} (Å)
[0,0,0] Γ_1^+ [Nb1:e:dsp] A1(a)	-0.63705	-0.45046	0.31853
[0,0,0] Γ_1^+ [O2:g:dsp] A1(a)	-0.41219	-0.29146	0.14573
[0,0,0] Γ_1^+ [O3:e:dsp] A1(a)	0.56210	0.39746	0.28105
[0,0,0] Γ_1^+ all	0.94429	0.66772	
[0,0,0] Γ_5^- [Li1:d:dsp] E(a)	0.0000	0.0000	0.0000
[0,0,0] Γ_5^- [Bi1:a:dsp] Eu(a)	-0.46107	-0.32603	0.32603
[0,0,0] Γ_5^- [Nb1:e:dsp] E(a)	-0.06753	-0.04775	0.03377
[0,0,0] Γ_5^- [O1:b:dsp] Eu(a)	0.01795	0.01269	0.01269
[0,0,0] Γ_5^- [O2:g:dsp] B2(a)	0.42192	0.29834	0.14917
[0,0,0] Γ_5^- [O2:g:dsp] B1(a)	-0.00486	-0.00344	0.00172
[0,0,0] Γ_5^- [O3:e:dsp] E(a)	-0.14640	-0.10352	0.07320
[0,0,0] Γ_5^- all	0.64571	0.45659	
[$\frac{1}{2}, \frac{1}{2}, 0$] X ₂ ⁺ [Li1:d:dsp] E(a)	-0.00378	-0.00267	0.00189
[$\frac{1}{2}, \frac{1}{2}, 0$] X ₂ ⁺ [O2:g:dsp] B2(a)	-0.67097	-0.47445	0.23722
[$\frac{1}{2}, \frac{1}{2}, 0$] X ₂ ⁺ [O2:g:dsp] B1(a)	0.00216	0.00153	0.00076
[$\frac{1}{2}, \frac{1}{2}, 0$] X ₂ ⁺ all	0.67098	0.47446	
[$\frac{1}{2}, \frac{1}{2}, 0$] X ₄ ⁻ [Bi1:a:dsp] Eu(a)	0.11613	0.08212	0.08212
[$\frac{1}{2}, \frac{1}{2}, 0$] X ₄ ⁻ [Nb1:e:dsp] E(a)	-0.04970	-0.03514	0.02485
[$\frac{1}{2}, \frac{1}{2}, 0$] X ₄ ⁻ [O1:b:dsp] Eu(a)	0.54320	0.38410	0.38410
[$\frac{1}{2}, \frac{1}{2}, 0$] X ₄ ⁻ [O2:g:dsp] A1(a)	0.60062	0.42470	0.21235
[$\frac{1}{2}, \frac{1}{2}, 0$] X ₄ ⁻ [O3:e:dsp] E(a)	-0.81899	-0.57911	0.40950
[$\frac{1}{2}, \frac{1}{2}, 0$] X ₄ ⁻ all	1.1587	0.81930	

Table S10. Distortion mode amplitudes extracted from the refined structure of LiBiNb₂O₇ (space group *B2cm*) compared to the *I4/mmm* symmetry aristotype structure.

NaBiNb ₂ O ₇			
Distortion mode	A _s	A _p	d _{max} (Å)
[0,0,0] Γ_1^+ [Nb1:e:dsp] A1(a)	-0.58470	-0.29235	0.20672
[0,0,0] Γ_1^+ [O2:g:dsp] A1(a)	-0.83339	-0.41669	0.20835
[0,0,0] Γ_1^+ [O3:e:dsp] A1(a)	1.1725	0.58623	0.41453
[0,0,0] Γ_1^+ all	1.5528	0.77638	
[0,0,0] Γ_4^- [O2:g:dsp] A1(a)	-0.34851	-0.17425	0.087130
[0,0,0] Γ_4^- all	0.34851	0.17425	
$[\frac{1}{2},\frac{1}{2},0]$ X ₂ ⁺ [Na1:d:dsp] E(a)	-0.06896	-0.03448	0.02438
$[\frac{1}{2},\frac{1}{2},0]$ X ₂ ⁺ [O2:g:dsp] B2(a)	-0.85046	-0.42523	0.21262
$[\frac{1}{2},\frac{1}{2},0]$ X ₂ ⁺ [O2:g:dsp] B1(a)	0.07662	0.03831	0.01916
$[\frac{1}{2},\frac{1}{2},0]$ X ₂ ⁺ all	0.85668	0.42834	
$[\frac{1}{2},\frac{1}{2},0]$ X ₃ ⁺ [Na1:d:dsp] B2(a)	0.14388	0.07194	0.05087
$[\frac{1}{2},\frac{1}{2},0]$ X ₃ ⁺ [Nb1:e:dsp] E(a)	0.07585	0.03793	0.02682
$[\frac{1}{2},\frac{1}{2},0]$ X ₃ ⁺ [O2:g:dsp] A1(a)	0.09308	0.04654	0.02327
$[\frac{1}{2},\frac{1}{2},0]$ X ₃ ⁺ [O3:e:dsp] E(a)	0.36470	0.18235	0.12894
$[\frac{1}{2},\frac{1}{2},0]$ X ₃ ⁺ all	0.41003	0.20502	
$[\frac{1}{2},\frac{1}{2},0]$ X ₂ ⁻ [Na1:d:dsp] E(a)	0.06896	0.03448	0.02438
$[\frac{1}{2},\frac{1}{2},0]$ X ₂ ⁻ [Bi1:a:dsp] A2u(a)	0.04329	0.02165	0.02165
$[\frac{1}{2},\frac{1}{2},0]$ X ₂ ⁻ [Nb1:e:dsp] A1(a)	0.21123	0.10562	0.07468
$[\frac{1}{2},\frac{1}{2},0]$ X ₂ ⁻ [O1:b:dsp] A2u(a)	0.02165	0.01082	0.01083
$[\frac{1}{2},\frac{1}{2},0]$ X ₂ ⁻ [O2:g:dsp] B2(a)	0.26816	0.13408	0.06704
$[\frac{1}{2},\frac{1}{2},0]$ X ₂ ⁻ [O3:e:dsp] A1(a)	0.17449	0.08725	0.06169
$[\frac{1}{2},\frac{1}{2},0]$ X ₂ ⁻ all	0.39252	0.19626	
$[\frac{1}{2},\frac{1}{2},0]$ X ₃ ⁻ [Na1:d:dsp] B2(a)	-0.14388	-0.07194	0.05087
$[\frac{1}{2},\frac{1}{2},0]$ X ₃ ⁻ [Bi1:a:dsp] Eu(a)	-0.23405	-0.11703	0.11703
$[\frac{1}{2},\frac{1}{2},0]$ X ₃ ⁻ [Nb1:e:dsp] E(a)	-0.21453	-0.10726	0.07585
$[\frac{1}{2},\frac{1}{2},0]$ X ₃ ⁻ [O1:b:dsp] Eu(a)	0.77148	0.38574	0.38574
$[\frac{1}{2},\frac{1}{2},0]$ X ₃ ⁻ [O2:g:dsp] A1(a)	0.47406	0.23703	0.11852
$[\frac{1}{2},\frac{1}{2},0]$ X ₃ ⁻ [O3:e:dsp] E(a)	-0.56697	-0.28348	0.20045
$[\frac{1}{2},\frac{1}{2},0]$ X ₃ ⁻ all	1.1238	0.56189	
[1,1,1] M ₅ ⁺ [Na1:d:dsp] E(a)	-0.03831	-0.01915	0.01354
[1,1,1] M ₅ ⁺ [Nb1:e:dsp] E(a)	0.04597	0.02298	0.01625
[1,1,1] M ₅ ⁺ [O2:g:dsp] B2(a)	0.02299	0.01150	0.00575
[1,1,1] M ₅ ⁺ [O2:g:dsp] B1(a)	0.06129	0.03064	0.01532
[1,1,1] M ₅ ⁺ [O3:e:dsp] E(a)	0.12259	0.06130	0.04334
[1,1,1] M ₅ ⁺ all	0.15131	0.07565	
[1,1,1] M ₅ ⁻ [Na1:d:dsp] E(a)	-0.03831	-0.01915	0.01354
[1,1,1] M ₅ ⁻ [Bi1:a:dsp] Eu(a)	-0.61112	-0.30556	0.30556
[1,1,1] M ₅ ⁻ [Nb1:e:dsp] E(a)	0.04674	0.02337	0.01653
[1,1,1] M ₅ ⁻ [O1:b:dsp] Eu(a)	-0.13003	-0.06502	0.06502
[1,1,1] M ₅ ⁻ [O2:g:dsp] B2(a)	-0.62061	-0.3103	0.15515
[1,1,1] M ₅ ⁻ [O2:g:dsp] B1(a)	0.04597	0.02298	0.01149
[1,1,1] M ₅ ⁻ [O3:e:dsp] E(a)	-0.05057	-0.02528	0.01788
[1,1,1] M ₅ ⁻ all	0.88536	0.44268	

Table S11. Distortion mode amplitudes extracted from the refined structure of NaBiNb₂O₇ (space group $P2_12_12_1$) compared to the $I4/mmm$ symmetry aristotype structure.

6. First-principles analysis of RbBiNb₂O₇ and LiBiNb₂O₇.

	Lattice parameters				Displacive symmetry adapted mode magnitudes				
	a (Å)	b (Å)	c (Å)	Vol(Å ³)	Γ_5^-	A_5^-	A_2^+	A_3^+	Γ_1^+
Parent (supercell)	22.311	5.450	5.450	662.750	-	-	-	-	-
VASP	22.490	5.360	5.432	654.836	0.81287	0.88286	1.07549	0.00921	0.32531
Experiment	22.422	5.382	5.452	657.984	0.82918	0.79429	0.73741	0.04633	0.40586

Table S12. Comparison between theoretical and experimentally synthesized structures of RbBiNb₂O₇ in the polar *I2cm* phase.

Space group	Source	<i>a</i> (Å)	<i>b</i> (Å)	<i>c</i> (Å)	Volume (Å ³)
<i>Bmcm</i>	PBEsol	5.5665	5.5620	20.0563	620.9755
<i>B2cm</i>	Experiment	5.4560	5.3415	20.8186	606.7211
	PBEsol	5.4456	5.3314	20.8069	604.0954

Table S13. Comparison between structures of LiBiNb₂O₇ in the listed space groups from our first-principles calculations (PBEsol) and experiment.

References

1. T. Zhu, G. Khalsa, D. M. Havas, A. S. Gibbs, W. Zhang, P. Halasyamani, N. A. Benedek and M. A. Hayward, *Chem. Mater.*, 2018, **30**, 8915-8924.
2. B. J. Campbell, H. T. Stokes, D. E. Tanner and D. M. Hatch, *J. Appl. Crystallogr.*, 2006, **39**, 607-614.
3. M. Jarvinen, *J. Appl. Crystallogr.*, 1993, **26**, 525-531.
4. P. W. Stephens, *J. Appl. Crystallogr.*, 1999, **32**, 281-289.
5. T. Zhu, T. Cohen, A. S. Gibbs, W. Zhang, P. S. Halasyamani, M. A. Hayward and N. A. Benedek, *Chem. Mater.*, 2017, **29**, 9489-9497.